International Journal of Fluid Machinery and Systems
Vol. 6, No. 2, April-June 2013

DOI: http://dx.doi.org/10.5293/IJFMS.2013.6.2.105
ISSN (Online): 1882-9554

Original Paper

Low Speed Design of Rear Rotor in Contra-Rotating Axial Flow Pump

Linlin Cao[1], Satoshi Watanabe[2], Simpei Momosaki[1], Toshiki Imanishi[1], Akinori Furukawa[3]

[1]Graduate School of Engineering, Kyushu University,
744 Motooka, Nishi-ku, Fukuoka, 819-0319, Japan,
linlin.cao@fcs.mech.kyushu-u.ac.jp, s.momosaki@fcs.mech.kyushu-u.ac.jp,
t.imanishi@fcs.mech.kyushu-u.ac.jp
[2]Department of Mechanical Engineering, Kyushu University,
744 Motooka, Nishi-ku, Fukuoka, 819-0319, Japan, fmnabe@mech.kyushu-u.ac.jp
[3]Oita National College of Technology,
1666 Maki, Oita, 870-0152, Japan, a-furukawa@oita-ct.ac.jp

Abstract

The application of contra-rotating rotors for higher specific speed pump has been proposed in our studies, which is in principle effective for reducing the rotational speed and/or the pump size under the same specification of conventional axial flow pump. In the previous experiments of our prototype, the cavitation inception at the tip region of the rear rotor rather than that of the front rotor and the strong potential interaction from the suction surface of the rear rotor blade to the pressure surface of the front one were observed, indicating the possibility to further improve the pump performance by optimizing rotational speed combination between the two rotors. The present research aims at the design of rear rotor with lower rotational speed. Considering the fact that the incoming flow velocity defects at the tip region of the rear rotor, an integrated inflow model of 'forced vortex' and 'free vortex' is employed. The variation of maximum camber location from hub to tip as well as other related considerations are also taken into account for further performance improvement. The ideas cited above are separately or comprehensively applied in the design of three types of rear rotor, which are subsequently simulated in ANSYS CFX to evaluate the related pump performance and therefore the whole low speed design idea. Finally, the experimental validation is carried out on one type to offer further proofs for the availability of the whole design method.

Keywords: contra-rotating rotors, blade design, cavitation, CFD.

1. Introduction

The axial flow pump with higher flow rate operation is increasingly required in drainage fields due to its advantages of the low cost and compact structure while it is also suffering the cavitation problem and efficiency deterioration as the high specific speed pump [1,2]. The contra-rotating axial flow pump with two rotors rotating reversely, offers a better solution for these fields [3,4]. In our previous experiments, it has been confirmed that, under the same specific speed, this type of pump reduces the head and the rotational speed of each rotor respectively, which brings about better cavitation performance and higher efficiency at the design point [3,4].

Given the same rotation speed of both rotors (N_f=N_r), the cavitation inception was observed in the tip region of the rear rotor rather than the front rotor at the off design conditions [4]. Regardless of the pressure rise of front rotor, the larger relative inflow velocity of rear rotor was found to mainly contribute to the early occurrence of cavitation, which indicates the possibility to further improve the cavitation performance by the optimized rotational speed combination of two rotors. In addition, it has been found from the instantaneous wall pressure measurements that a strong potential interaction from the suction surface of the rear rotor blade to the pressure surface of the front one appears due to higher stagger installation of the rear rotor blades [4]. These facts imply the effectiveness of rotational speed optimization between front and rear rotors.

Received July 17 2012; revised January 18 2013; accepted for publication February 28 2013: Review conducted by Prof. Hyung-Hee Cho. (Paper number O13004S)
Corresponding author: Satoshi Watanabe, Professor, fmnabe@mech.kyushu-u.ac.jp

This paper was presented at 5th International Symposium on Fluid Machinery and Fluids Engineering, October 24-27, 2012, Jeju, Korea.

The present research aims at the design of the new rear rotor with reduced rotational speed for more favorable performances of contra-rotating axial flow pump. After the determination of the rotational speed for both rotors in order to reduce relative inlet velocity and stagger angle of rear rotor blade, three types of rear rotors are designed with thinner blade profile, positive incidence angle and longer chord length, as well as smaller stagger angle. Because the exiting flow from the front rotor is observed to defect at the tip region in our previous experiments [5], the integrated model of 'forced vortex' and 'free vortex' for the inflow velocity distribution is adopted in the new rotor design presented here. The idea of variable maximum camber location from hub to tip of blade is also employed to reduce the shock-loss around the blade leading edge and the secondary flow while for the former rotors the maximum camber location was kept as 40% from the leading edge to the chord length through the whole blades. These design ideas are comprehensively or separately applied in different rotors, which are simulated in ANSYS CFX to make a comparison on related performances and therefore to estimate the availability of those design ideas. One of the designed rear rotors, in which both the integrated model for the inflow velocity distribution and the variable maximum camber location were applied, was found to highly satisfy the design specification with the highest efficiency in the numerical simulation. Then, this type of rotor was manufactured and the experimental validation has been carried out to offer further proofs for the availability of the whole design method.

2. Design basis

As the higher relative velocity with low flow angle at the inlet of rear rotor blade with larger stagger angle causes the cavitation inception in the rear rotor tip region and the strong potential interaction between two rotors, the rotational speed optimization is required in the new rotor design, which will be described in Sec. 3. Other defects observed in the experiments of the previously designed rotors are also considered in this section, which are listed as follows:

2.1. Observed outflow velocity distribution of front rotor

The circumferential-averaged axial (V_z) and circumferential (V_θ) components of absolute velocity at the inlet of rear rotor are illustrated in Fig. 1, where r_c denotes the radius at the inner surface of casing. As shown in Fig. 1, measured axial velocity depicted by solid symbols significantly deviates from that under the 'Free vortex' design (blue curve) especially at the tip region, while the circumferential velocity slightly increased from the previous design condition in this region. The tip leakage vortex of the front rotor must be the main cause of the axial velocity defect, which has also been proved in the CFD simulation of the case with and without tip clearance. As described in Fig. 1, the 'normal' model with the tip clearance of 1mm (green curves) shows a larger velocity deviation than the 'noclearance' model (red curves) especially at the tip position.

Since the tip blade profile greatly influences on the rotor efficiency, with the consideration of the actual inlet flow of rear rotor, the model of 'forced vortex' described in the following sections is applied to express the inflow boundary condition in the design of new rear rotor.

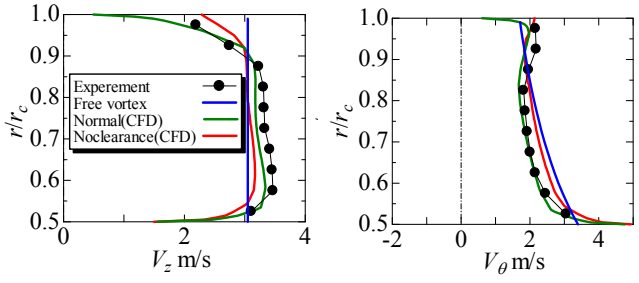

Fig. 1 Inflow velocity distribution of rear rotor at the design condition (Q=70L/s N_f=1225 rpm).

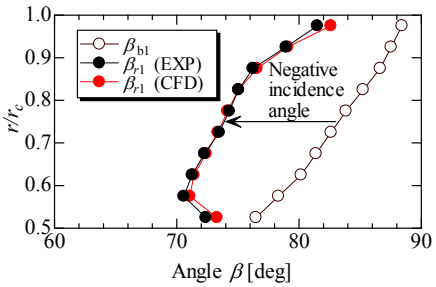

Fig. 2 The incidence angle distribution of the rear rotor at the design condition (Q=70L/s N_f=N_r=1225 rpm).

2.2. Negative incidence angle of rear rotor

For the existing rear rotor (RR2 type) designed by the conventional way with the profile series of NACA44**, the profile dimension of which will be described in Table 3, the measured and numerically calculated relative inflow angles are plotted in Fig. 2 in comparison with the designed inlet blade angle β_{b1}.

The negative incidence angle i (i=β_{r1}-β_{b1}) is observed, which is known as unfavorable to inlet shock-loss and cavitation performance, due to which the stagnation point locates on the blade suction surface near the blade leading edge [6]. The positive incidence angle is considered as one of the most important design principles during the design of the new rear rotor.

3. Determination of blade parameters

The thickness of the new rear rotor is determined by the NACA4* series which is employed in the design of previous rear rotor as the following eq. (1):

$$\frac{y_t(x)}{l} = 5\frac{t}{l}\left\{a_0\sqrt{\frac{x}{l}} + a_1\frac{x}{l} + a_2\left(\frac{x}{l}\right)^2 + a_3\left(\frac{x}{l}\right)^3 + a_4\left(\frac{x}{l}\right)^4\right\} \tag{1}$$

While a new quadratic parabola for the camber angle is adopted as eq. (2):

$$\theta(x) = ax^2 + bx + c \tag{2}$$

Several new ideas for performance improvement are applied in the detail parameter determination which are absence in the design of the previous ones.

3.1 Determination of design rotational speed

Given the same rotational speed of both front and rear rotors (N_f=N_r), the relative inflow velocity W_{r1} of rear rotor is in general larger than the relative inflow velocity W_{f1} of front rotor, resulting in higher required NPSH ($NPSH_r$) than that of front rotor, despite that the inlet static pressure of rear rotor is increased by the head-rise of front rotor. It seems reasonable to delay the cavitation inception of rear rotor by optimizing the combination of rotational speed of two rotors, which results in '$NPSH_{rf}$> $NPSH_{rr}$' where the subscripts *f* and *r* denote the front and rear rotor respectively. In addition, the decreasing rotational speed of rear rotor also brings about the increase in the relative inflow velocity angle to weaken the blade row interaction.

For the front rotor:

$$NPSH_{rf} = \frac{V_z^2}{2g} + \lambda_f \frac{W_{f1}^2}{2g} \tag{3}$$

For the rear rotor:

$$NPSH_{rr} = \frac{V_z^2}{2g} + \frac{V_{\theta f2}^2}{2g} + \lambda_r \frac{W_{r1}^2}{2g} - H_f \tag{4}$$

Given the condition of $NPSH_{rf}$> $NPSH_{rr}$, $\lambda_f = \lambda_r$, $W_f = W_r$, the following eq. (5) could be obtained by eq. (3) and eq. (4):

$$H_f - \frac{V_{\theta f2}^{\ 2}}{2g} > 0 \tag{5}$$

Combined with the equation of Euler Head, the rotational speeds of both rotors can be described as follows:

$$N_f = \frac{60}{\pi D_t}\sqrt{\frac{gH/\eta}{1-\left(1-\psi_f/\eta_f\right)^2}}$$

$$N_r = \frac{60}{\pi D_t}\left(1-\frac{\psi_f}{\eta_f}\right)\sqrt{\frac{gH/\eta}{1-\left(1-\psi_f/\eta_f\right)^2}}$$

Given the total pump head of *H*=4m and design flow rate of *Q*=70 L/s as the previous rotors, and the measured peak efficiency point of the front rotor (at *Q*=63 L/s for N_f=1225 rpm) [5], the optimized rotational speeds combination are obtained as:

N_f=1311 rpm; N_r=1123 rpm

3.2 Determination of blade profile parameters

3.2.1 Flow angles

The positive incidence angle through the whole blade is considered as one of the most important design principles. The specification of inflow velocity, based on the actual inflow distribution, enables the realization of the proposed relative inflow angle and the positive incidence angle. Since, in the previous experiments, the measured velocity distribution at the outlet of the rear rotor, i.e. at the inlet of the rear rotor, has been found to be deviated from the assumed distribution of "free vortex", the new "integrated model" is herein proposed, where the "forced vortex" distribution is assumed near the tip region. This integrated model is shown in Table 1.

Table 1 Integrated inflow velocity profile

Position	V_θ	V_z
$r< r_m$	$rV_\theta = K$	$V_z = C_1$
$r> r_m$	$\frac{V_\theta}{r-r_h} = \Omega$	$V_z = \sqrt{C_2 - 2\Omega^2(r-r_h)^2}$
$r= r_m$	$\frac{K}{r_m(r_m-r_h)} = \Omega$	$C_1 = \sqrt{C_2 - 2\Omega^2(r_m-r_h)^2}$

The joint section between free and forced vortex-type flow distributions is set at the position of r_m=0.0875r_c, where the velocity is experimentally confirmed to start defecting regardless of the rotational speed. As shown in Fig. 3, the velocity distribution expressed by the new integrated model shows a good agreement with the simulated outflow velocity distribution (with normal tip clearance as 1mm) of front rotor.

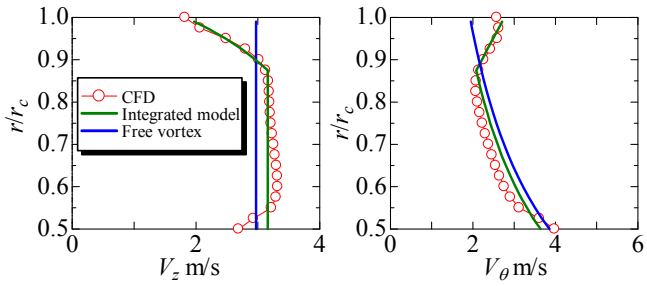

Fig. 3 Velocity distributions under different models at the new design speed (Q=70L/s N_f=1311 rpm).

Given the assumption of no swirl at the rear rotor outlet ($V_{\theta r2}$=0), the inlet and outlet relative flow angles could be determined based on the velocity distribution as follows:

$$\beta_{r1} = \tan^{-1}\left(\frac{r\omega_r + V_{\theta r1}}{V_z}\right) \qquad \beta_{r2} = \tan^{-1}\left(\frac{r\omega_r}{V_z}\right)$$

The incidence angle is set as consistently i=2° through the whole blade from hub to tip. The deviation angle at the outlet of rear rotor is determined according to the following empirical equation eq. (6) obtained from the parameter study using CFD, where $\Delta\beta$ denotes the turning angle of the flow through the blade passage:

$$\delta = \Delta\beta + 13.05\left(\frac{x_f}{l} - 0.4\right) \tag{6}$$

3.2.2 Maximum camber location

Since Zangeneh [7] has indicated that the secondary flow could be well controlled with the blade designed as leading edge loaded at tip and trailing edge loaded at hub, the idea of variable maximum camber position is adopted in the new rear rotor RR3 design. Compared to the RR2 with the consistent maximum camber x_f/l positioned at 40% to chord length over the whole blade span, the x_f/l of RR3 adopts 40% at the tip and smoothly shifts into 60% at the hub.

3.2.3 Other parameters

For the favorable performance, the RR3 type is designed with smaller thickness to reduce the blockage effect, larger length as well as larger solidity to relief the tip leakage vortex, and smaller stagger angle to decrease the influence from the low pressure region of the suction side onto the flow field of front rotor.

3.3 Detail parameters of three new types of RR3

Three new types of rear rotor RR3 are designed as described in Table 2. The detailed profile parameters designed at 5 radial sections for the RR3 as well as the previous rear rotor RR2 are listed in Table 3 to make a clearer description of the differences among them.

Table 2 The application of the design ideas in 3 types of RR3

Type	Inflow velocity model	Maximum camber location
RR3-Z	Integrated	Variable
RR3-F	Free vortex	Variable
RR3-40	Integrated	Consistence

As described in Table 3, compared to the RR2 type, all of three types of RR3 are designed with higher solidity, larger attack angle α and smaller stagger angle γ except for the hub section of RR3-Z and RR3-F. Compared to RR3-40, the maximum camber location on the hub section of the RR3-Z and RR3-F is designed as x_f/l 60% therefore more closed to the trailing edge, resulting in larger stagger angles and smaller attack angle on the hub section. Totally the RR3-40 type is designed with the largest average attack angle covering the major blade span, while the RR3-F type with the smallest at the tip region.

Table 3 The profile parameters of the RR2 and RR3 types

Blade Profile	Section	1 (Hub)	2	3	4	5 (Tip)
	D [m]	0.100	0.125	0.150	0.175	0.198
RR2	σ (l/t)	0.840	0.780	0.720	0.660	0.600
	x_f/l	0.40	0.40	0.40	0.40	0.40
	γ [°]	64.24	68.86	72.54	75.34	77.56

	α [°]	5.17	3.08	1.56	0.53	-0.23
RR3-Z	σ (l/t)	1.008	0.936	0.864	0.792	0.720
	x_f/l	0.60	0.55	0.50	0.45	0.40
	γ [°]	64.95	67.05	69.73	72.33	71.88
	α [°]	3.414	3.793	3.292	2.529	8.613
RR3-F	σ (l/t)	1.008	0.936	0.864	0.792	0.720
	x_f/l	0.60	0.55	0.50	0.45	0.40
	γ [°]	65.44	67.26	69.73	72.15	74.24
	α [°]	3.734	4.270	3.890	3.236	2.512
RR3-40	σ (l/t)	1.008	0.936	0.864	0.792	0.720
	x_f/l	0.40	0.40	0.40	0.40	0.40
	γ [°]	58.71	65.14	69.47	72.53	71.88
	α [°]	9.654	5.703	3.552	2.329	8.613

4. Performance evaluation by CFD

The internal flow with newly designed three types of rear rotor are simulated in ANSYS CFX 13 to make a comparison on related performance and therefore to estimate the availability of the design ideas.

Our previous numerical simulation for RR2 rotors [6] has shown that, even at the design flow rate, the transient simulation with whole blade passage models of both front and rear rotors is necessary for quantitative evaluations of pump performances. In addition, the total number of the calculation nodes up to 1.1 million for the whole passages, where 10 nodes are distributed between the blade tip end and the casing wall, has been found to be sufficient to reproduce the overall flow field inside the blade passages of the front and rear rotors as well as the detailed flow structures such as the tip leakage flow. Then, in the present study, the transient numerical simulation with the whole passage model is again carried out for the newly designed three rotor pairs, RR3-Z, RR3-F and RR3-40.

In the simulation, the so-called 'transient rotor-stator model' implemented in ANSYS CFX is used at the interface between computational domains of the front and rear rotors. As the boundary conditions, the mass flow rate is specified at the inlet located $4D_c$ upstream of the front rotor, and the static pressure at the outlet located $1.3D_c$ downstream of the rear rotor. All the walls are treated as non-slip wall. The turbulence model of 'Shear Stress Transport (SST)' is employed. The time step is set to be less than that corresponding to 0.5 degree of the rotation of rotors, and the time averaged data after, at least, four revolutions of each rotor are used for the performance evaluation.

4.1 Hydraulic performance comparisons

Figure 4 compares the heads and the efficiencies of front and rear rotors as well as total ones between four combinations of rotors RR2, RR3-Z, RR3-F and RR3-40.

For the evaluation of head-rises of front and rear rotor in each pair, H_f and H_r, time-averaged values of the casing wall static pressure differences between the upstream and downstream of the rotor are calculated, and the difference of dynamic head based on the axial velocity component are taken into the corresponding measured static head difference. This procedure is the same for that done in the experimental evaluations [6]. Then total head is calculated by $H=H_f+H_r$. The hydraulic efficiencies of each rotor, η_f and η_r, are calculated as the ratio of the corresponding water power $\rho gQH_{f,r}$ to the shaft power $L_{sh,f,r}=2\pi T_{f,r}N_{f,r}/60$, where $T_{f,r}$ is a time-averaged torque of each front and rear rotor. Then the total hydraulic efficiency is calculated by $\eta=\rho gQH/(L_{sh,f}+L_{sh,r})$.

From Fig. 4, although the identical front rotor is used for all the combinations, the head and the efficiency of front rotor can be found to be increased with the newly designed RR3 rear rotor from that with RR2 rotor, which is simply due to the difference of operating condition of front rotor, namely lower flow coefficient with higher efficiency and larger rotational speed in RR3 types.

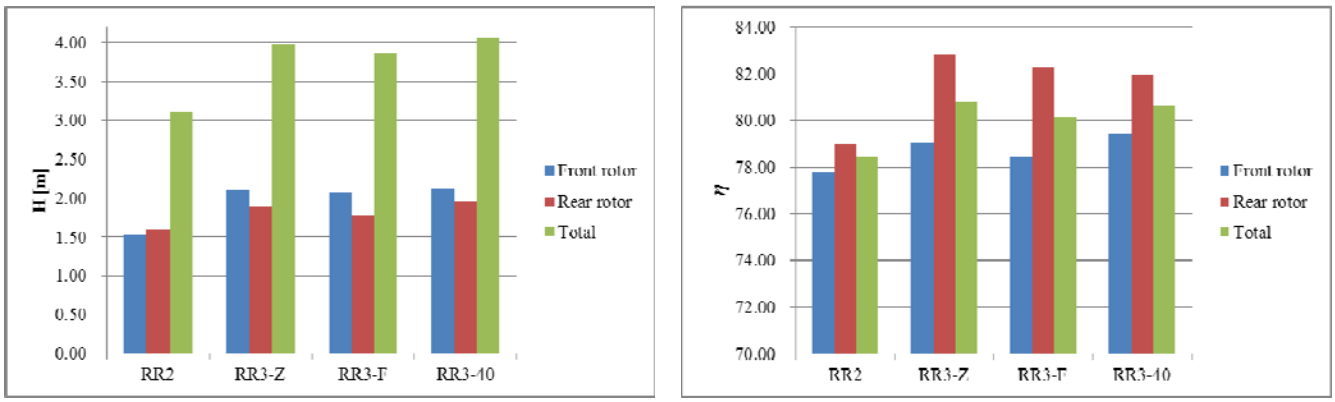

(a) Head of three types of RR3 and RR2 (b) Efficiency of three types of RR3 and RR2

Fig. 4 Numerical simulated performance of RR3 and RR2

In rear rotors, with considering several factors into the design, the new types of RR3 rear rotor show significant performance improvements from the previous RR2 rotor.

The RR3 types offer a significant head increase than the RR2 type. The type of RR3-Z and RR3-40, both of which designed under the integrated model of forced and free vortex for the inflow velocity distribution, offer the favorable head performance around 2.1m therefore the total pump head is highly close to the design condition, while the RR3-40 designed with the largest attack angle could reach the highest total head as 4.07m. In spite of a head increase than the RR2 type, the RR3-F, in which only the model of 'free vortex' is applied, performs inferior than the other two types, which means a probable loss at the tip position due to the unreal assumption of the inflow velocity distribution during the design process.

In spite of a lower head than other two types of RR3, RR3-F still offers a favorable head and efficiency than the RR2 type, which means, besides the integrated model for the inflow velocity, other considerations such as longer chord length, positive incidence angle and so on also take effects on the improvement of internal flow situation and the loss reduction in the rear rotor. On the other hand, although the RR3-40 type shows the largest total pump head within the three types of RR3 rear rotor, the consumption of shaft power which corresponds roughly to Euler's head increases, results in lower efficiency than the other two types. The absence of the control in secondary flow, which is applied in the other two rotors, probably causes the additional increase of shaft power, contributing to the lower efficiency of RR3-40 type.

The rear rotor optimization significantly contributes to the efficiency improvement of RR3-F and –Z types as shown in Fig. 4. Among the newly designed rear rotors, the RR3-Z type applied both the integrated model of inflow velocity distribution and the variable maximum camber location gains the highest efficiency with 82.8%. This fact indicates the importance to pay more attention to the blade profile design at the tip region and the loss reduction through the blade profile optimization.

4.2 Cavitation performance comparison

A series of transient simulations with the multiphase model considering cavitation are necessary to discuss about the cavitation performance of rotors, whereas in the present paper, we describe the possibility of cavitation in terms of cavitation inception with the minimum pressure obtained by single-phase transient simulations. The required NPSH ($NPSH_r$) based on the cavitation inception can be estimated by the following Eq. (7).

$$NPSH_r=(P_{Tinlet}-P_{min})/\rho g \tag{7}$$

Where P_{Tinlet} denotes the total pressure at the inlet of the pump, i.e. at the inlet of front rotor, and the P_{min} as the lowest static pressure on the blade profile. Although the location of minimum pressure often appears in the tip leakage vortices and/or on the tip surface of blade, the minimum value on the suction surface of blade is employed for NPSH evaluation, since it is believed to be directly related with the blade cavitation performance.

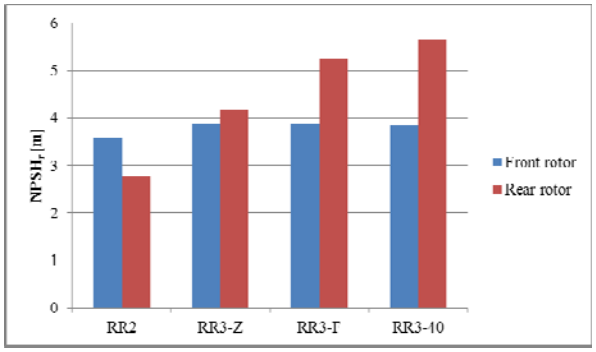

Fig. 5 $NPSH_r$ for three types of RR3 and RR2 by CFD

Figure 5 compares the values of $NPSH_r$ of front and rear rotors between four combinations of rotors RR2, RR3-Z, RR3-F and RR3-40.We can see that the required NPSH of front rotor is higher with the all types of RR3 rear rotor than that with the RR2 type, indicating that the cavitation performance of front rotor in terms of cavitation inception becomes worse with the RR3 types. This is simply due to the relative velocity increase with the increase of rotational speed of front rotor.

On the other hand, for the rear rotors, the required NPSH of all types of RR3 is also higher than that of RR2 type, in spite of the reduced rotational speed of RR3 rear rotor. This is because we have designed RR3 types with the positive incidence angle, resulting in the large angle of attack with the increased negative peak pressure. Among three types of RR3 rear rotors, the RR3-Z is turned out with the best cavitation performance in terms of cavitation inception. The RR3-40 type has been designed with the largest attack angles as described in Table 3, resulting in worse cavitation performance than the RR3-Z type. For the RR3-F type, although the design attack angle is the smallest, the free vortex inflow is assumed, which is far from the real inflow especially for the tip region. Inappropriate flow angle due to 'free vortex' assumption is believed to lead coincidently the unfavorable pressure distribution around the blade, deteriorating the cavitation performance of RR3-F rear rotor.

A lower $NPSH_r$ has been shown for the RR2 type than the RR3 types in terms of cavitation inception, however, the RR2 type with the large negative incidence angle would suffer from the cavitation on the pressure side as well as on the suction side as the NPSH is further reduced, which is considered to cause easily head breakdown of the rotor. We expect that, in terms of performance breakdown due to cavitation, the RR3 types with small positive incidence angles are favorable. We would like to investigate the effectiveness of new RR3 design in terms of cavitation breakdown by transient cavitation CFD simulation, which will be discussed in our future publications.

5. Experimental validation with RR3-Z type

We have manufactured the RR3-Z rear rotor, which has been shown by CFD with the best hydraulic and cavitation performances among the newly designed RR3 types. Performance test has been carried out, results of which along with those of RR2 type are shown in Fig. 6. In the figure, the values obtained by CFD numerical simulations in the previous section are also plotted, from which we can confirm the validity of our numerical approach.

As shown in Fig. 6 (a), the head of front rotor is totally increased with the RR3 type in the whole range of flow rate, which is mainly due to the increase of rotational speed of front rotor. The maximum efficiency point moves to the larger flow rate as expected, whereas the efficiency in the partial flow rate range is slightly increased due to the weakened interaction of the rear rotor blades with the reduced rotational speed.

On the other hand, the head of RR3 rear rotor is comparable to that of RR2 type, despite of the reduced rotational speed of RR3 type, as shown in Fig. 6 (b). Appropriate design of RR3 type especially near the tip region contributes to the favorable head characteristics as well as to the efficiency increase. A positive incidence angle at the design condition of RR3 makes the maximum efficiency point move to the larger flow rate, then the loss increases at the partial flow rates, resulting in the efficiency deterioration in this flow rate range.

In total, the rotor pair with RR3 shows benefits in the pump head and efficiency at the higher flow rate as shown in Fig.6 (c), which also offers us a possibility to improve these characteristics at the off design conditions by the additional rotational speed controls of rotors.

Totally, according to the results from both experiments and numerical simulations, the newly designed contra-rotating rotor pairs offer favourable performances highly meet the design specification, and the CFD simulation with the rotor interface as 'transient rotor-stator' reliably predicted the performances of the contra-rotating pump despite of the complicated rotor interaction and vortices structure inside.

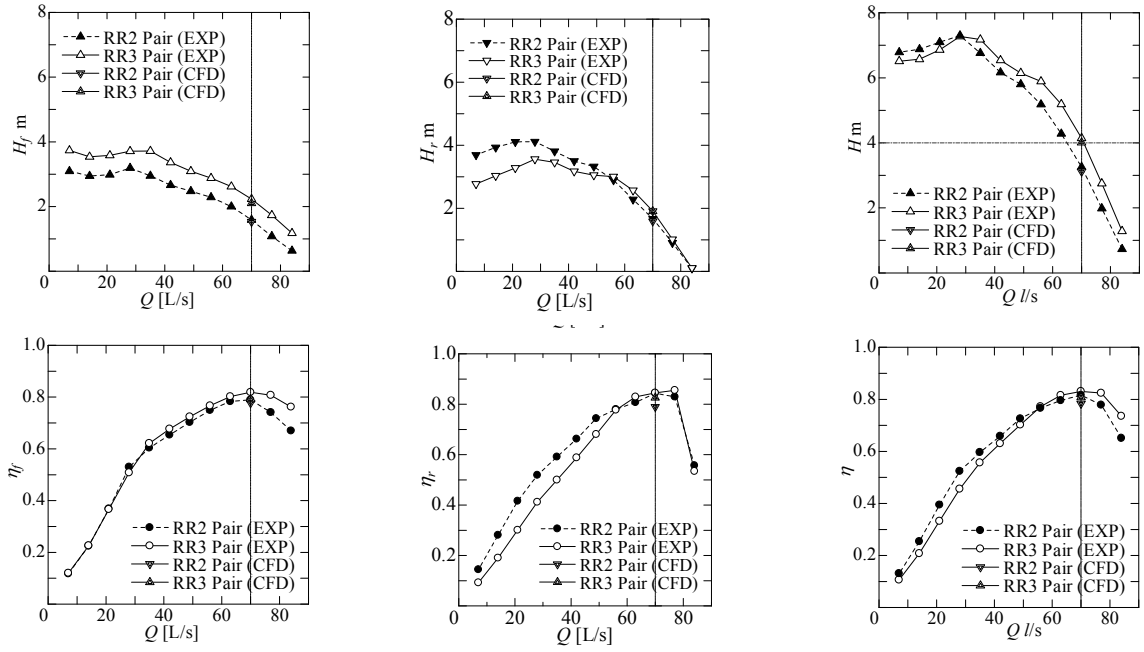

(a) Head and efficiency of front rotor

(b) Head and efficiency of rear rotor

(c) Head and efficiency of whole pump

Fig. 6 Measured head and efficiency characteristics of three types of RR3 and RR2 type

6. Conclusion

For the wider application of the contra-rotating axial flow pump, this research focused on the design method of the new type of rear rotor by rotational speed optimization for further improved performance.

Our conclusions are briefly summarized as follows:

1) The integrated model with forced vortex at the tip region, which models the real inflow velocity distribution of rear rotor, is effective for the rotor design giving higher efficiency.
2) The RR3 type designed with the variable maximum camber location shows higher efficiency than that with the consistent maximum camber location, which offers us a profile design guideline for the reduction of the secondary flow and the related losses.
3) The optimized rotational speed combination between the rotor pairs and the integrated considerations such as thinner blade profile, positive incidence angle and longer chord length take obvious effects on the improvement of cavitation inception performance.

Despite of no superiority in the cavitation inception is shown for the RR3 compared with the RR2, the better cavitation performance is expected since the cavitation on the blade surface of the RR3 is supposed to develop much slower than RR2 and limit only on the suction surface due to the profile optimization, resulting in better cavitation performance than the RR2 type. A

series of transient simulations with the multiphase model is now in preparation for the further research on the cavitation performance of these rotors, the results of which will be discussed in our future papers.

Acknowledgements

The authors would like to thank to Torishima Pump Mfg. Co., Ltd. for manufactures of test rotors. This study was partly supported by KAKENHI (23360086).

Nomenclature

D_c	Casing diameter [m]	α	Attack angle [°]
H	Head [m]	β	Relative flow angle [°]
i	Incidence angle [°]	β_b	Blade profile angle [°]
L_{sh}	Shaft power [kW]	γ	Stagger angle [°]
l	Chord length [m]	δ	Deviation angle [°]
N	Rotational speed [rpm]	σ	Solidity [-]
$NPSH_r$	Required Net Positive Suction Head [m]	η	Hydraulic efficiency [-]
P	Pressure [Pa]		
Q	Volumetric flow rate [L/s]		
R	Radius [m]		
r_c	Casing radius [m]		**Subscripts**
r_h	Hub radius [m]	1	At inlet
x_f	The max. camber location from the leading edge [m]	2	At outlet
T	Torque [Nm]	f	Front rotor
V_z	Axial velocity in absolute frame [m/s]	r	Rear rotor
V_θ	Circumferential velocity in absolute frame [m/s]		
W_1	Relative inflow velocity [m/s]		

References

[1] A. Wada, S. Uchida, 1993, “Improvement of Performance for Higher Specific Speed Axial-Flow Pump,” Torishima Review (in Japanese) Vol. 13, pp. 32-35.
[2] J.W. White, J.G. Purnell, J.G. Stricker, 1993, “In-Line Submersible Pump,” Proc. 2nd ASME Pumping Machinery Symposium, paper No. 246.
[3] A. Furukawa, Y. Cao, K. Okuma, S. Watanabe, 2000, “Experimental Study of Pump Characteristics of Contra-Rotating Axial Flow Pump,” Proc. 2nd International Symposium on Fluid Machinery and Fluid Engineering, Beijing, China, pp. 245-252.
[4] A. Furukawa, T. Shigemitsu, S. Watanabe, 2007, “Performance Test and Flow Measurement on Contra-rotating Axial Flow Pump,” Thermal Science, Vol. 16, pp. 7-13.
[5] S. Momosaki, S. Usami, K. Okuma, S. Watanabe, A. Furukawa, 2010, “Experimental Study on Rotational Speed Control of Contra-Rotating Axial Flow Pump,” Proc. of 3rd Asian Joint Workshop on Thermophysics and Fluid Science, Matsue, Japan, paper No. JP-02.
[6] S. Momosaki, S. Usami, S. Watanabe, A. Furukawa, 2010, “Numerical Simulation of Internal Flow in a Contra-rotating Axial Flow Pump,” 25th IAHR Symposium on Hydraulic Machinery and Systems, Timisoara, Romania.
[7] M. Zangeneh, 1991, “A Compressible Three-dimensional Design Method for Radial and Mixed Flow Turbomachinery Blades,” International Journal of Numerical Methods in Fluids, Vol. 13, pp. 599-624.